AGU PUBLICATIONS

Geochemistry, Geophysics, Geosystems

TECHNICAL REPORTS: METHODS

10.1002/2016GC006339

Key Points:
- We offer practical approach using conventional equipment to better define paramagnetic fabric by LT-AMS measurements
- By using silicon sheet protection we manage to achieve high measuring accuracy and to obtain reliable LT-AMS fabric
- Temperature analysis suggests that LT-AMS measurements in air amplifies paramagnetic susceptibility by a factor of ~3.2 in chalks

Correspondence to:
R. Issachar,
ranissachar@gmail.com

Citation:
Issachar, R., T. Levi, V. Lyakhovsky, S. Marco, and R. Weinberger (2016), Improving the method of low-temperature anisotropy of magnetic susceptibility (LT-AMS) measurements in air, *Geochem. Geophys. Geosyst.*, *17*, doi:10.1002/2016GC006339.

Received 3 MAR 2016
Accepted 5 JUN 2016
Accepted article online 8 JUN 2016

Improving the method of low-temperature anisotropy of magnetic susceptibility (LT-AMS) measurements in air

R. Issachar[1,2], T. Levi[2], V. Lyakhovsky[2], S. Marco[1], and R. Weinberger[2,3]

[1]Department of Geosciences, Tel Aviv University, Tel Aviv, Israel, [2]Geological Survey of Israel, Jerusalem, Israel, [3]Department of Geological and Environmental Sciences, Ben-Gurion University of the Negev, Beer-Sheva, Israel

Abstract This study examines the limitations of the method of low-temperature anisotropy of magnetic susceptibility (LT-AMS) measurements in air and presents technical improvements that significantly reduce the instrumental drift and measurement errors. We analyzed the temperature profile of porous chalk core after cooling in liquid nitrogen and found that the average temperature of the sample during the LT-AMS measurement in air is higher than 77K and close to 92K. This analysis indicates that the susceptibility of the paramagnetic minerals are amplified by a factor ~3.2 relative to that of room temperature AMS (RT-AMS). In addition, it was found that liquid nitrogen was absorbed in the samples during immersing and contributed diamagnetic component of $\sim -9 \times 10^{-6}$ SI to the total mean susceptibility. We showed that silicone sheet placed around and at the bottom of the measuring coil is an effective thermal protection, preventing instrument drift by the cold sample. In this way, the measuring errors of LT-AMS reduced to the level of RT-AMS, allowing accurate comparison with standard AMS measurements. We examined the applicability of the LT-AMS measurements on chalk samples that consist <5% (weight) of paramagnetic minerals and showed that it helps to efficiently enhance the paramagnetic fabric. The present study offers a practical approach, which can be applied to various types of rocks to better delineate the paramagnetic phase using conventional equipment.

1. Introduction

Anisotropy of magnetic susceptibility (AMS) reveals various geological processes such as deformation [*Oertel*, 1983; *Borradaile and Alford*, 1988; *Borradaile*, 1991; *Borradaile and Henry*, 1997; *Parés et al*., 1999; *Borradaile and Jackson*, 2004; *Soto et al*., 2007; *Levi and Weinberger*, 2011; *Cifelli et al*., 2013; *Levi et al*., 2014; *Braun et al*., 2015; *Issachar et al.,* 2015], sedimentation [*Borradaile and Tarling*, 1981; *Pennec et al*., 1998; *Gautam and Rösler*, 1999; *Ort et al*., 2003; *Petronis and Geissman*, 2009] and flow [*Cagnoli and Tarling*, 1997; *Zanella et al*., 1999; *Palmer and MacDonald*, 1999; *Rochette et al*., 1999; *Morris*, 2000; *Wang et al*., 2001; *Porreca and Mattei*, 2003; *Levi et al*., 2006a,b; *LaBerge et al*., 2009; *Dedzo et al*., 2011]. The AMS measurement averages the orientation-distribution of all minerals and associated diamagnetic, paramagnetic, and ferromagnetic phases. Hence, it is essential to develop techniques to identify the contribution of each of the magnetic phases to the total AMS.

Measuring the AMS at low temperature has a great potential to characterize the paramagnetic fabric [*Martin-Hernandez and Ferre*, 2007]. Low temperature AMS (LT-AMS) enhances the effect of paramagnetic minerals. According to Curie-Weiss law the volume susceptibility k increases as temperature decreases (T) as $k=C/(T-\theta)$; where C is the specific mineral Curie constant and θ is the paramagnetic Curie temperature, which is zero for pure paramagnetic materials [e.g., *Cullity,* 1972]. Accordingly, at 77K (boiling temperature of liquid nitrogen) the paramagnetic susceptibility increases by a factor of ~3.8 relative to room temperature AMS (RT-AMS) at 295K. Diamagnetic susceptibility does not show temperature dependence [*Cullity*, 1972], whereas ferromagnetic minerals often show susceptibility changes at low temperatures, (e.g., Verwey transition in magnetite-titanomagnetite or Morin transition in hematite [*Verwey*, 1939; *Morin*, 1950; *Morrish*, 1994; *Cowgill et al*., 2004; *Özdemir et al*., 2008]). Nevertheless, in rocks with very low ferromagnetic components relative to the paramagnetic component, the paramagnetic minerals dominantly govern the susceptibility changes at low temperatures. Consequently, the measurements at LT-AMS amplify the contribution of the

paramagnetic minerals in the rock sample. Hence, the LT measurements may help in separating the AMS into its paramagnetic, diamagnetic and ferromagnetic components [*Martin-Hernandez and Ferre*, 2007].

LT-AMS measurements are carried out by two different approaches: In approach (1) the measurement is carried out while immersing the sample in liquid nitrogen [*Parés and van der Pluijm*, 2002]. In approach (2) the sample is cooled in liquid nitrogen and subsequently measured in air [*Lüneburg et al*., 1999]. Approach (1) has the advantage of keeping the sample at homogeneous and constant temperature but requires a custom-made holder, which is not suitable for most susceptibility meters. In approach (2) the measurement procedure is much simpler but an increase in temperature during the measurement is inevitable.

Parés and van der Pluijm [2002, 2014] have demonstrated the applicability of the LT-AMS for characterization of phyllosilicate fabrics. They used approach (1) with a custom-made dewar glass flask, which was placed into a thin styrofoam jacket to protect the instrument from cooling. They placed the flask inside a 'Sapphire Instruments' susceptibility meter with a large coil (internal diameter of 45 mm).

Schmidt et al. [2007] introduced a modification of approach (1), in which the LT-AMS measurements were conducted in high field up to 1.5 Tesla using a torque magnetometer. They also used a custom dewar (cylindrical Pyrex, double-walled, silver coated) allowing measurements while immersing the sample in liquid nitrogen. In this way, they have managed to separate the paramagnetic contribution from the total AMS of synthetic calcite–muscovite aggregates. The main advantage of the torque method is that the high field allows measurements above saturation of most ferromagnetic minerals and, hence, subtracting their contribution to the total AMS. *Schmidt et al*. [2007] reported that the sensitivity of instrument is 3×10^{-8} SI and the measuring time is around 1 hour for each sample. A disadvantage of torque measurements is that only the deviatoric susceptibility tensor is determined, while the mean susceptibility could not be resolved [*Jelinek*, 1985].

Lüneburg et al. [1999] were the first to report on LT-AMS measurements of slates in air (approach 2) using an AGICO Kappabridge with a manual holder method. Each sample was immersed in liquid nitrogen for 30 minutes before the first measurement, and repeatedly for 1 minutes between each of the following 15 position measurements. *Oliva-Urica et al*. [2010] and *Oliva-Urica and Roman-Berdiel* [2010] followed *Lüneburg et al*. [1999] and measured LT-AMS of marls and phyllites, modifying the measuring protocol for the use of the spinning sample holder in the Kappabridge.

Many studies [*Cifelli et al*., 2004, 2005, 2009, 2011; *Debacker et al*., 2009; *Oliva-Urcia et al*., 2012, 2013, 2011; *Soto et al*., 2012, 2014; *Garcia-Lasanta et al*., 2013; *Haerinck et al*., 2013; *Izquierdo-Llavall et al*., 2013; *García-Lasanta et al*., 2014; *Santolaria et al*., 2015] followed *Lüneburg et al*. [1999], *Oliva-Urica et al*. [2010], and *Oliva-Urica and Roman-Berdiel* [2010] protocols, characterizing the LT-AMS of rocks, mainly due to the standardization of the equipment used and the popularity of the Kappabridge susceptibility meter.

2. Challenges in LT-AMS Measurements

Although low-field LT-AMS measurements in air are frequently used, the implementation of the method encounters obstacles that can lead to large measurement errors and questionable interpretations.

This method tackles four main obstacles:

1. Estimating and considering the temperature profile in the sample during measurement [*Parés and van der Pluijm*, 2002, 2014; *Martin-Hernandez and Ferre*, 2007]. After cooling in liquid nitrogen, the sample is taken out for measurement in air, and immediately the temperature within the sample starts to increase heterogeneously from 77K to room temperature (295K). The temperature distribution in the sample volume and its changes with time depends on the physical properties of the studied rock and the geometry of the sample. Hence, estimating the temperature profile of the sample during measurement is not straightforward and hampers the possibility to simply refer to the paramagnetic amplification factor.
2. Enlarged errors due to temperature increase during measurement. In the slowly spinning specimen method the directional susceptibilities are measured for 5 or 8 revolutions of the specimen around each spinning axis [*Jelinek*, 1995; *Gee et al*., 2008]. Susceptibilities are recorded in 64 positions per revolution and averaged for all revolutions [*Gee et al*., 2008]. The signal between two revolutions may decrease and

Table 1. Sample Weights Before and After Immersion in Liquid Nitrogen (LqNi)

Sample	Volume (cm^3)	Weight Before Immersion (g)	Weight After Immersion (g)	Weight Difference (g)	LqNi Volume (cm^3)	Susceptibility Due to LqNi ($\times 10^{-6}$ SI)
MR-2	10.8	16.3	19.6	3.3	4.1	−9.0
MR-12	10.8	17.0	20.4	3.4	4.2	−9.1
MR-18	10.8	16.1	19.5	3.4	4.2	−9.2
AD-7	10.3	15.2	18.3	3.1	3.8	−8.8
AD-15	10.3	14.5	17.7	3.2	3.9	−8.9
AD-17	10.3	13.4	16.9	3.5	4.4	−10.0
AD-18	10.3	13.6	16.7	3.1	3.8	−8.8
AD-19	10.3	13.6	17.2	3.6	4.5	−10.2

accordingly the measuring error might increase, due to the increase of the sample temperature during the measurement.

3. Reducing instrument drift that is caused by the low temperature of the sample. The cold sample is placed in the coil leads to cold air convection and drift of the electrical components. This leads to significant errors and halt of measurements.
4. Correcting additional and artificial susceptibility values that are introduced by absorption of liquid nitrogen into the sample. Liquid nitrogen has low diamagnetic susceptibility (k_m, the mean susceptibility $= -23.5 \times 10^{-6}$ SI), which might add negative susceptibility to the total AMS.

In this study, we examined the limitation and precision of the LT-AMS measurements in air and present technical improvements that reduce the instrument drift and measurement errors. The applicability of the technical solutions were tested on chalk samples of the Maresha and Adulam Formations, which contain small amounts of paramagnetic minerals, mainly palygorskite and smectite (<5% by weight) [*Nathan and Flexer*, 1977], high porosity of >20% [*Palchik and Hatzor*, 2002], and low mean susceptibilities (this study).

3. Correction for Absorption of Liquid Nitrogen

To determine the addition of liquid nitrogen susceptibility in the rock samples, the weight of three samples of Maresha and five samples of Adulam were measured before and after 50 minute immersion in liquid nitrogen (Table 1). The weight of the sample immediately after immersion was ∼20% higher than the initial weight and then steadily decreased. Almost all the absorbed liquid nitrogen evaporated after 120 s and the sample returned to its original weight. The weight after immersion reported in Table 1 is the average weight between 10 and 20 s after immersion. Then, the additional susceptibility values were calculated, and the LT-AMS measurements corrected (see chapter 6). These tests showed that for the present samples the liquid nitrogen adds diamagnetic susceptibility of $\sim -9 \times 10^{-6}$ SI to the total LT-AMS.

4. Sample Temperature Profile

We analyzed the temperature profile of a standard cylinder sample with radius of 12.5 mm (r_0) and height of 25.4 mm. The temperature was measured by a thermocouple in three holes drilled in the sample at $r=0$, $r=0.7 \cdot r_0$ and $r=0.85 \cdot r_0$ (Figure 1). The sample with the thermocouple in its central hole was immersed in liquid nitrogen for 50 minutes and then removed out to the air. The temperature was recorded every 30 s for 30 minutes afterward. In order to estimate the sample temperature profile we solved an analytical model of conductive heat transfer and calibrated it using the measured temperatures. We treated the cylinder as a sphere, and solved the heat equation for spherical symmetric temperature distribution $T(r,t)$:

$$\frac{\partial T}{\partial t} = \alpha \frac{1}{r^2} \frac{\partial}{\partial r} \left(r^2 \frac{\partial T}{\partial r} \right) \quad \text{for } 0 < r < r_0, \tag{1}$$

where t is the time, r is the radius and α is thermal diffusivity. Equation 1 considers the conductive heat transfer and neglects the advection, which is associated with the absorbed liquid nitrogen motion and evaporation. These processes might be important during the early stage of heating, and will be estimated in comparison with the direct temperature measurements.

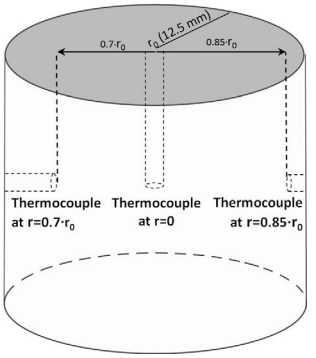

Figure 1. Temperature measurements in a representative cylindrical sample.

Constant initial temperature, T_i=77K, was set as the initial condition:

$$T(r,0)=T_i. \quad (2)$$

Heat flux at the surface was set as the boundary condition:

$$-k\frac{\partial T}{\partial r}=h(T-T_\infty) \quad \text{for } r=r_0, \quad (3)$$

where k is thermal conductivity, h is the heat transfer coefficient for the system and T_∞ =295K is the final temperature. Introducing dimensionless variables, $\theta=(T-T_\infty)/(T_i-T_\infty)$, $\tau=\alpha t/r_0^2$ and $\xi=r/r_0$, the solution is [*Ozisik*, 1993]:

$$\theta(\tau,\xi)=\sum_{n=1}^{\infty} C_n e^{-\lambda_n^2\tau}\frac{1}{\xi}\sin(\lambda_n\xi), \quad (4)$$

where λ_n are the roots of:

$$1-\lambda_n\cot(\lambda_n)-B_i=0 \quad (5)$$

and:

$$C_n=4\frac{-\sin(\lambda_n)+\cos(\lambda_n)\lambda_n}{(\sin(2\lambda_n)-2\lambda_n)\lambda_n}, \quad (6)$$

where $B_i=hr_0/k$, known as the Biot Number. To obtain greater accuracy in the initial times, 16 terms were considered (n=1 *to* 16).

Figure 2 shows the results of the temperature measurements over time. For the associated calculated curves, values of α and B_i were obtained by using a best fit procedure between the measured data and the calculated solution (equations (4)–(6)) at r=0, r=0.7·r_0 and r=0.85·r_0. The calculated temperature profile using the conductive heat flux model (equation 1) with $\alpha=0.8\cdot10^{-7}$ (m^2/s) and B_i=4 fits well the measured temperatures starting from 120 s after immersion (Figure 2a). Since almost all of the absorbed liquid nitrogen evaporates during the first 120 s (as described in the previous section), the conductive heat transport dominates the heating at relatively late stages. However, during the first 120 s, the measured temperatures near the sample surface slightly deviate from the calculated curve (Figure 2b). This early stage discrepency is probably due to motion and evaporation of the absorbed liquid nitrogen.

Figure 3 shows the calculated temperature curves, as a function of the sample volume, after 10 and 20 s (mean susceptibility measurement last 10–20 s after the sample is removed from liquid nitrogen bath, see section 5 below). The average temperatures are 87K and 96K respectivly and accordingly, the average

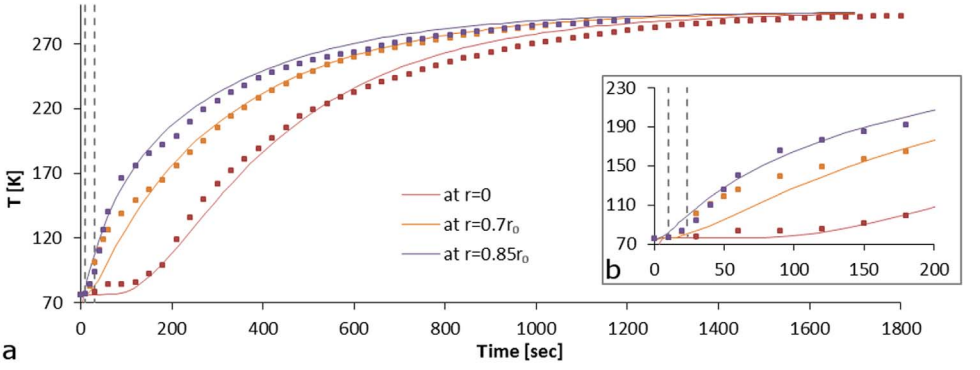

Figure 2. Temperature profiles in cylindrical chalk samples with 12.5mm radius (r_0). The samples measured at air for initial temperature T_i=77K. Squares represent measured values at r=0 (red), r=0.7·r_0 (yellow) and r=0.85·r_0 (purple). Curves represent the best fit calculated solution of the heat-eqution. Dash gray lines represent the time range during the AMS measurement (10–20 s). (a) Results obtained for 1800 s. (b) enlargment of the first 200 s.

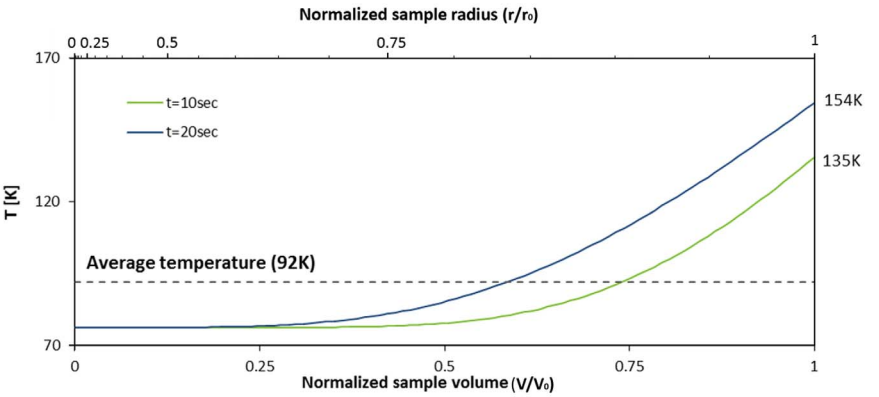

Figure 3. Calculated temperature profile along the sample volume after 10 (green) and 20 s (blue). For 10 and 20 s curves temperature at the center is 77K and at surfuce 135K and 154K, respectivly. The dashed line is the average temperature between 10 and 20 s.

temperature of the sample for the time period 10–20 s after imerssion is 92K. We note that the model provides a reasonable estimate for the sample temperature during LT-AMS which is certainly higher than 77K and close to 92K. Following the Curie-Weiss law, the paramagnetic amplification factor for the LT-AMS measurements in air is practically 3.2 (295K divided by 92K).

5. LT-AMS Measurements in Air

LT and RT AMS were measured at low magnetic field of 300 A/m with a KLY-4S Kappabridge (AGICO Inc.) using the spinning sample method [*Jelinek*, 1995] at the Geological Survey of Israel. Directional susceptibilities measurements lasts ~20 s, and mean susceptibility (k_m) ~10 s. Another ~10 s are required to fix the sample in the holder, i.e., the measurements of directional susceptibilities last 10–30 s and of mean susceptibility 10–20 s after the sample is removed from liquid nitrogen bath.

During the LT-AMS measurements in air, the measurement errors increased dramatically due to instrument drift (see section 2). We adopted the solution suggested in previous studies [e.g., *Soto et al*., 2014] and wait 10 minutes between measurements, allowing the instrument recovery. Nevertheless, the errors on the LT-AMS measurements have remained large. To overcome this obstacle, we tested several improvements that could isolate the coil from excessive cooling (e.g., isolating the sample with a styrofoam jacket, gas circulation). We found that a thin silicone sheet (1.5 mm) made of high quality LSR silicone was very effective for thermal protection (LSR is an industrial technique of injection molding of liquid silicone rubber, commonly used in cookware). The silicone sheet was placed around and at the bottom of the measuring coil (Figure 4). To obtain reliable holder corrections, the holder with the silicone protection was measured separately before measurements. We found that the silicone sheet protection reduced the measuring errors significantly from 265.91 to 15.33 $\times 10^{-9}$ SI, the latter value is comparable to that of the RT-AMS measuring errors (Figure 5).

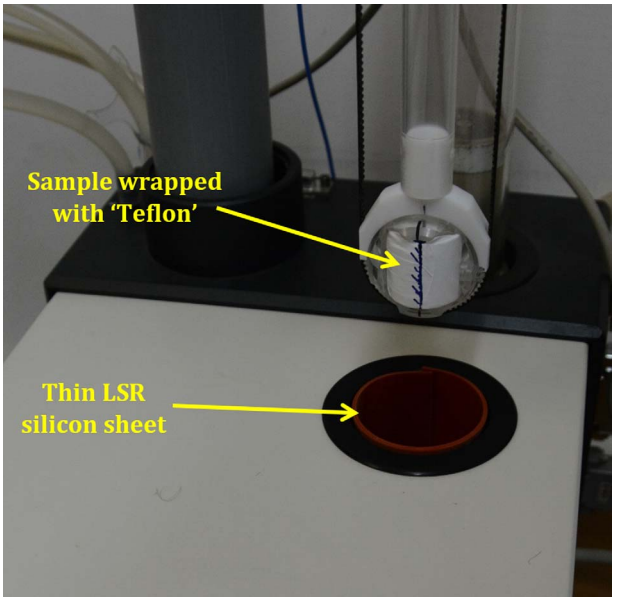

Figure 4. LT-AMS measurements setup using the AGICO Inc. KLY-4S Kappabridge. The yellow arrows show the sample covered with the 'Teflon' protection and the thin silicone sheet inserted into the measuring coil.

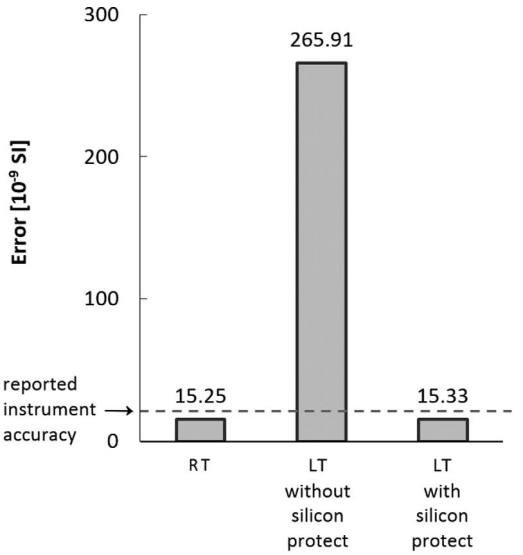

Figure 5. Errors of axial measurments (in average) presented in coloumn diagram from left to right: RT-AMS measurement, LT-AMS measurements without silicone protection and LT-AMS with measurements silicone protection. Dashed line shows the accuracy of the instrument reported for axial measurements (KLY-4S Kappabridge Manual, AGICO Inc.).

We also noticed that during the LT-AMS measurements, an ice layer was formed around the cold sample immediately after removing it from the liquid nitrogen bath. This ice layer affected the accuracy of the measurements but could be prevented by wrapping the samples with a thin polytetrafluoroethylene ('Teflon') layer (Figure 4), reducing significantly the ice condensation around the sample during measurements.

6. Application

To test the applicability of the above improvements, the RT-AMS and LT-AMS of 19 samples of Adulam and Maresha chalks were measured and compared (Table 2). Figure 6a shows the k_m values of LT ($LT\text{-}k_m$) versus that of RT ($RT\text{-}k_m$). The high positive linear correlation ($R^2=0.94$) indicates that $RT\text{-}k_m$ and $LT\text{-}k_m$ growth is related to increase in paramagnetic mineral contents. The point on the graph where k_m values of LT and RT are equal represents a hypothetical k_m value that excludes the contribution of paramagnetic minerals, namely the k_m of diamagnetic and ferromagnetic phases. The linear regression suggests that k_m values of LT and RT measurements are equal for -11.3×10^{-6} SI (Figure 6a). This value is close to the susceptibility of single calcite crystal ($k_m \approx -12.87 \times 10^{-6}$ SI) [*Nye*, 1957; *Owens and Rutter*, 1978; *Schmidt et al*., 2006], suggesting the dominancy of diamagnetic phase and the negligible ferromagnetic contribution to k_m in the samples. Figure 6b presents $|LT\text{-}k_m/RT\text{-}k_m|$ versus $RT\text{-}k_m$ values (see example in Ciffeli et al. [2005]). For pure paramagnetic sample, $|LT\text{-}k_m/RT\text{-}k_m|$ should be ~3.2 (see section 3). For the present samples, the $|LT\text{-}k_m/RT\text{-}k_m|$ ratios range between 5 and 10, with inverse correlation to positive values of $RT\text{-}k_m$. This confirms that the diamagnetic phase has a significant contribution to k_m, because the susceptibility of a sample at RT is the sum of the ferromagnetic, paramagnetic and diamagnetic components (k_f, k_p and k_d respectively) [*Henry and Daly*, 1983; *Hrouda et al*., 2000]:

$$RT\ \ k_m = c_f k_f + c_p k_p + c_d k_d \equiv K_f + K_p + K_d, \tag{7}$$

where c_f, c_p and c_d are the respective percentages.

Further, at LT, the paramagnetic phase is amplified by factor of ~3.2:

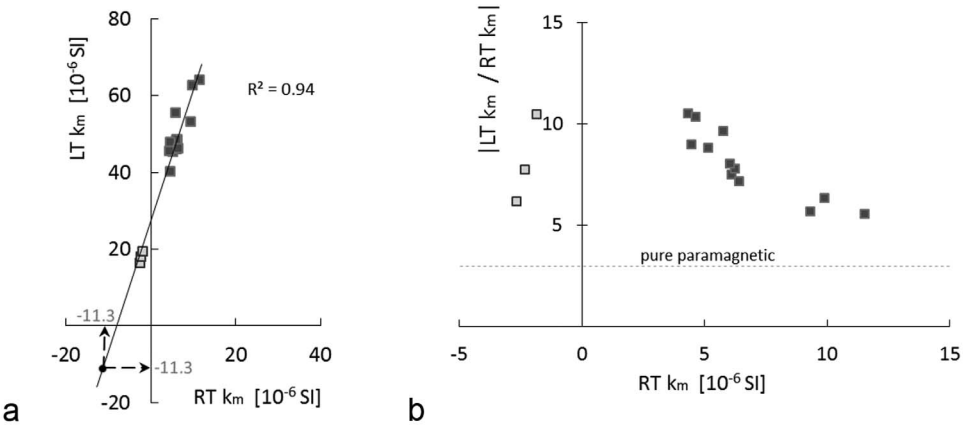

Figure 6. (a) LT-k_m versus RT-k_m. (b) |LT-k_m/RT-k_m| versus RT-k_m. dash line represents the paramagnetic amplification factor of the measurements (3). Maresha and Adulam samples marked by filled and empty sequares, respectively.

Table 2. Low-Field RT-AMS and LT-AMS Parameters of Maresha (MR) and Adulam (AD) Chalks

	RT-AMS				LT-AMS				
Sample	k_m ($\times 10^{-6}$ SI)	T	Pj	Normalized Principal Magnitudes ($k_1/k_2/k_3$)	k_m ($\times 10^{-6}$ SI)	T	Pj	Normalized Principal Magnitudes ($k_1/k_2/k_3$)	$\lvert\frac{LT\ k_m}{RT\ k_m}\rvert$
MR-1	5.14	0.50	1.16	1.06/1.02/0.91	45.39	0.12	1.009	1.004/1.000/0.995	8.8
MR-2	6.11	0.56	1.22	1.07/1.03/0.89	45.95	0.52	1.012	1.005/1.002/0.993	7.5
MR-4	4.48	0.29	1.28	1.11/1.02/0.87	40.29	0.61	1.034	1.013/1.006/0.981	9.0
MR-5	4.33	0.40	1.19	1.07/1.02/0.91	45.57	0.28	1.004	1.002/1.000/0.998	10.5
MR-6	3.78	0.36	1.06	1.03/1.01/0.96	44.42	−0.31	1.004	1.002/0.999/0.998	11.7
MR-7	6.25	0.85	1.09	1.03/1.02/0.95	48.58	0.11	1.007	1.003/1.000/0.996	7.8
MR-8	5.09	−0.16	1.12	1.06/0.99/0.95	44.71	−0.25	1.006	1.003/0.999/0.997	8.78
MR-9	6.05	0.84	1.15	1.04/1.03/0.92	48.57	0.65	1.008	1.003/1.001/0.996	8.0
MR-12	4.63	0.57	1.15	1.05/1.02/0.92	47.95	−0.03	1.004	1.002/1.000/0.998	10.4
MR-13	11.53	0.35	1.32	1.12/1.02/0.85	64.20	0.28	1.022	1.001/1.002/0.988	5.6
MR-14	9.88	−0.08	1.31	1.14/0.99/0.87	62.71	−0.17	1.007	1.004/0.999/0.997	6.3
MR-15	7.56	−0.20	1.29	1.14/0.98/0.88	59.30	−0.35	1.003	1.002/1.000/0.998	7.8
MR-16	5.76	0.21	1.21	1.09/1.01/0.90	55.59	0.22	1.008	1.004/1.001/0.996	9.6
MR-17	6.42	0.22	1.32	1.13/1.01/0.86	46.18	0.76	1.014	1.005/1.003/0.992	7.2
MR-18	9.33	0.10	1.22	1.09/1.00/0.90	53.15	0.12	1.006	1.003/1.000/0.997	5.7
MR-19	9.80	0.43	1.19	1.07/1.02/0.90	54.30	−0.34	1.011	1.006/0.999/0.995	5.5
AD-7	−2.65	-	-	-	16.38				6.2
AD-15	−2.32	-	-	-	18.04				7.8
AD-17	−1.85	-	-	-	19.33				10.5

$$LT\ \ k_m = c_f k_f + 3.2 \cdot c_p k_p + c_d k_d \equiv K_f + 3.2 \cdot K_p + K_d \tag{8}$$

Therefore, the ratio between LT and RT is:

$$\frac{LT\ \ k_m}{RT\ \ k_m} = \frac{K_f + K_d + 3.2 \cdot K_p}{K_f + K_d + K_p} \tag{9}$$

If $(K_f + K_d)$ is a negative number, i.e., diamagnetic dominancy, then LT/RT ratio is lower than the paramagnetic amplification factor, ($\frac{LT\ \ k_m}{RT\ \ k_m} > 3.2$). In contrast, if $(K_f + K_d)$ is a positive number, i.e., ferromagnetic dominancy, then LT/RT ratio is higher than the paramagnetic amplification factor, ($\frac{LT\ \ k_m}{RT\ \ k_m} < 3.2$).

The RT-AMS fabric shows well grouped k_3 axes while k_1 and k_2 axes are scattered and form a well-defined inclined plane (Figure 7a). The 95% confidence ellipses of k_1 and k_2 axes are large and overlapped. The LT-AMS fabric is divided into two well defined groups based on the orientation of susceptibility axes. In Group A, which includes most of the samples, the AMS fabric is quite similar to that of the RT-AMS with slightly better separation of k_1 and k_2 axes, expressed by narrower 95% confidence ellipses (Figure 7b). In Group B, the AMS fabric is different from that of the RT-AMS fabric. This group is characterized by well grouped AMS axes, whereas k_3 orientations approximately related by a ~90° rotation around a vertical axis with respect to k_3 orientations in the RT-AMS fabric (Figure 7b). Figures 7c and 7d show the AMS shape parameter ($T = 2\ln(k_2/k_3)/\ln(k_1/k_3) - 1$ [*Hrouda*, 2004]) versus the corrected anisotropy degree, ($P_j = \exp\sqrt{2\sum(\ln k_i - \ln k_m)^2}$; i=1 to 3, k_m is the mean susceptibility [*Jelinek*, 1981]). In the RT-AMS P_j values range from 1.06 to 1.3 and T generally changes from oblate ($T=+1$) to neutral ellipsoid ($T=0$) with increase in P_j (Figure 7c). On the other hand, in the LT-AMS the P_j values are much lower, ranging from 1.004 to 1.04, where no correlation between T and P_j is obtained (Figure 7d). To better understand the source of the change in *Pj* values at LT a further investigation is required [*Almqvist et al.*, 2010], which is beyond the scope of this paper.

7. Discussion

In order to overcome the kappabridge drift when cold samples are measured, we tested a suitable thermal protection, which (1) fits the 2 mm gap between the holder and the coil, and (2) has a weak

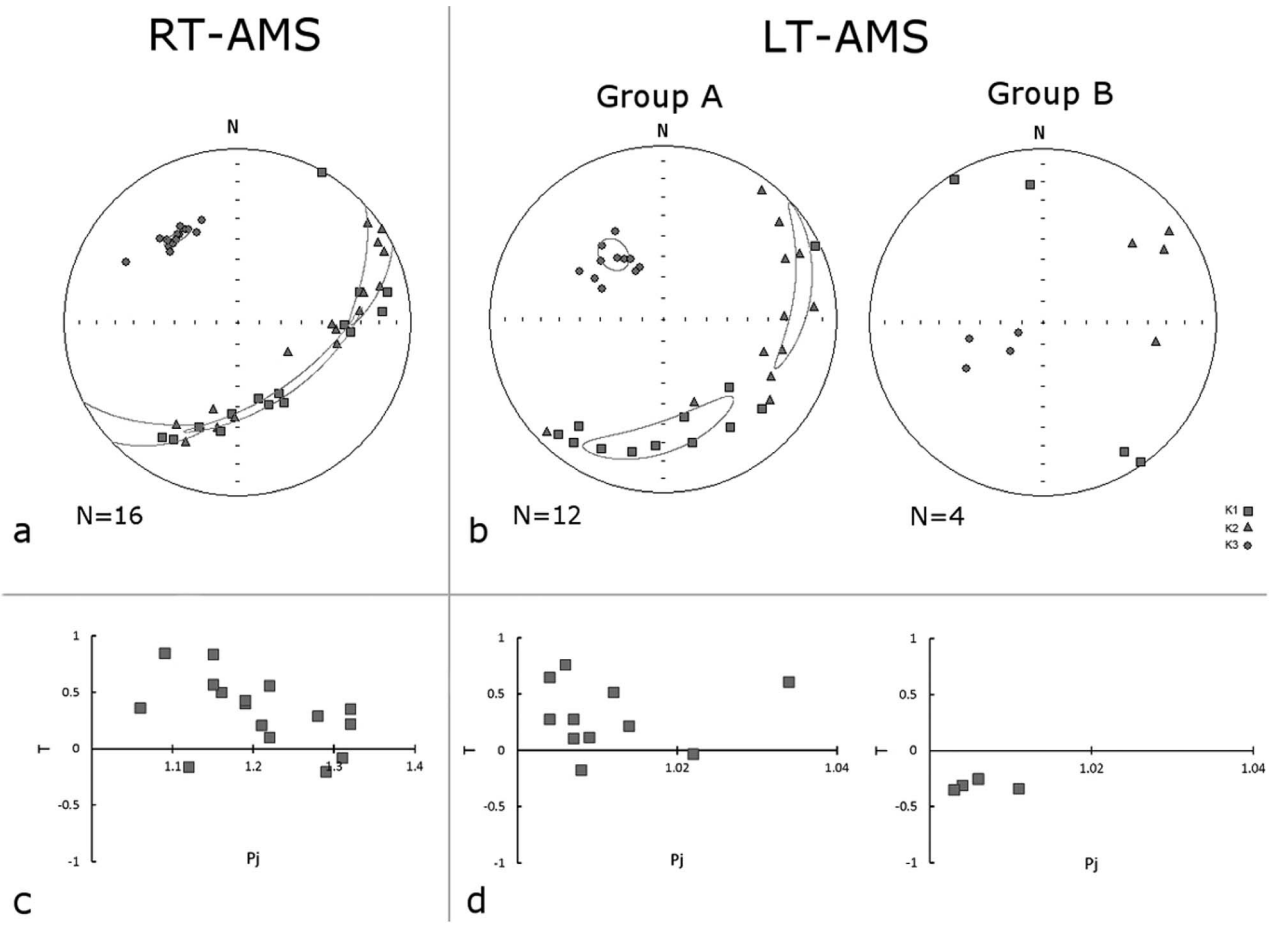

Figure 7. Magnetic fabrics of RT-AMS and LT-AMS measurements for Mearsha samples. (a and b) Lower-hemisphere, equal-area projection of AMS principal axis and their 95% confidence ellipses. (c and d) shape anisotropy (T) versus corrected anisotropy degree (Pj).

magnetic response that does not interfere with the measurements. We found that high quality LSR silicone sheet is efficient thermal insulator. The susceptibility of LSR silicone is $\sim 90 \times 10^{-6}$ SI, but has negligible contribution when placed around the coil. Another advantage to using the LSR silicone sheet protection is that it can easily be removed, allowing quick switching between RT and LT-AMS measurements. We show that by using this protection the measurement errors of LT-AMS decrease significantly, and are similar to that of RT-AMS errors (Figure 5). This allows us to achieve a reliable comparison between LT and RT fabrics.

In order to assess the temperature heterogeneity within the sample and determine the paramagnetic amplification factor, we calculated the temperature profiles within the rock volume (see section 4). We calibrated the conductive heat transfer model using temperature measurements of one representative sample. If needed it is possible to calibrate the model based on more than one representative sample. The analysis shows that after the sample is removed from the liquid nitrogen bath to air, the upper bound for the sample temperature during LT-AMS measurements is 92K. This value is higher than the 77K assumed in most studies that use LT-AMS measurements in air. These differences are expressed by differences in the paramagnetic amplification factor, which is $\sim$3.8 and $\sim$3.2 at 77K and 92K, respectively. This indicates that the theoretical paramagnetic amplification factor is reduced by $\sim$15% for practical LT-AMS measurements in air. The small measurement errors suggest that the concern of enlarged errors due to temperature increase during measurement (see section 2) is insignificant and, hence, the fabric measured by the LT-AMS method in air is reliable. The tested samples in this study represent an extreme case, in which they have low susceptibility values (k_m ranges between 4 and 10×10^{-6} SI) and >20% porosity. We found that the additional susceptibility due to liquid nitrogen absorption is $\sim -9 \times 10^{-6}$ SI. Hence, the addition of the diamagnetic

susceptibility of the liquid nitrogen to the AMS in rock samples with weak susceptibility values should not be overlooked. In rocks with high susceptibility values this addition may be less significant.

The paramagnetic amplification factor and the addition of liquid nitrogen susceptibility reported in this study were tested only on chalk. In rocks with high thermal diffusivity, the temperature increase rate in the sample is expected to be higher and as a result, the paramagnetic amplification factor will reduce significantly. Therefore, in order to obtain reliable results by LT-AMS measurements in air for other rock types, it is recommend determining the temperature profile and liquid nitrogen absorption for each rock type specifically, following the procedure presented in this study.

8. Conclusions

1. Using LSR silicone protection in the instrument coil reduces the high measuring errors caused by excessive cooling of the instrument to normal. This improvement helps to obtain reliable results in LT-AMS measurements in rocks containing $<$10% of paramagnetic content, and to compare them to RT-AMS measurements.
2. The paramagnetic amplification factor of LT-AMS measurements in air for the tested chalks is $\sim$3.2 (T=92K), which is lower by 15% compared with the theoretical value of $\sim$3.8 calculated for liquid nitrogen temperature (T=77K).
3. Liquid nitrogen absorption in low susceptibility and porous rocks adds significant component of diamagnetic susceptibility to the LT measurements. This artificial susceptibility component can be corrected by weighting the samples before and after the immersion in liquid nitrogen.
4. The present study offers a practical approach to improve the accuracy of the low-temperature AMS measurements using conventional equipment. The suggested approach can be applied to various types of rocks in order to better define their paramagnetic phase.

Acknowledgments
This study was supported by grants from the Israel Science Foundation grant 5411245/11 to RW, Israel Science Foundation Center of Excellence grant 1436/14 to SM, and the Israeli Ministry of National Infrastructures, Energy and Water Resources. We thank Ruth Soto and Josep Parés for their useful advice during the course of this study. We also thank Mike Jackson and Bjarne Almqvist for their very constructive reviews, which helped us to improve the manuscript considerably. All the data used for this study are accessible by contacting the authors at ranissachar@gmail.com.

References

Almqvist, B. S. G., M. Herwegh, V. Schmidt, T. Pettke, and A. M. Hirt (2010), Magnetic susceptibility as a tool to study deformed calcite with variable impurity content, *Geochem. Geophys. Geosyst.*, *11*, Q01Z09, doi:10.1029/2009GC002900.

Borradaile, G. J. (1991), Corralation of strain with anisotropy of magnetic-susceptibility (AMS), *Pure Appl. Geophys.*, *135*(1), 15–29, doi:10.1007/bf00877006.

Borradaile, G. J., and B. Henry (1997), Tectonic applications of magnetic susceptibility and its anisotropy, *Earth Sci. Rev.*, *42*(1-2), 49–93.

Borradaile, G. J., and M. Jackson (2004), Anisotropy of magnetic susceptibility (AMS): magnetic petrofabrics of deformed rocks, *Geol. Soc. Spec. Publ.*, *238*, 299–360.

Borradaile, G. J., and D. H. Tarling (1981), The influence of deformation mechanisms on magnetic fabrics in weahly deformed rocks, *Tectonophysics*, *77*(1-2), 151–168, doi:10.1016/0040-1951(81)90165-7.

Borradaile, G. J. J., and C. Alford (1988), Experimental shear zones and magnetic fabrics, *J. Struct. Geol.*, *10*(8), 895–904, doi:10.1016/0191-8141(88)90102-2.

Braun, D., R. Weinberger, Y. Eyal, S. Feinstein, Y. Harlavan, and T. Levi (2015), Distinctive diamagnetic fabrics in dolostones evolved at fault cores, the Dead Sea Transform, *J. Struct. Geol.*, *77*, 11–26, doi:10.1016/j.jsg.2015.05.007.

Cagnoli, B., and D. H. Tarling (1997), The reliability of anisotropy of magnetic susceptibility (AMS) data as flow direction indicators in friable base surge and ignimbrite deposits: Italian examples, *J. Volcanol. Geotherm. Res.*, *75*(3-4), 309–320, doi:10.1016/S0377-0273(96)00038-8.

Cifelli, F., M. Mattei, A. M. Hirt, and A. Gunther (2004), The origin of tectonic fabrics in "undeformed" clays: The early stages of deformation in extensional sedimentary basins, *Geophys. Res. Lett.*, *31*, L09604, doi:10.1029/2004GL019609.

Cifelli, F., M. Mattei, and M. Chadima (2005), The origin of tectonic lineation in extensional basins: combined neutron texture and magnetic analyses on "undeformed" clays, *Earth Planet. Sci. Lett.*, *235*(1), 62–78.

Cifelli, F., M. Mattei, M. Chadima, S. Lenser, and A. M. Hirt (2009), The magnetic fabric in "undeformed clays": AMS and neutron texture analyses from the Rif Chain (Morocco), *Tectonophysics*, *466*(1-2), 79–88, doi:10.1016/j.tecto.2008.08.008.

Cifelli, F., L. Minelli, F. Rossetti, G. Urru, and M. Mattei (2011), The emplacement of the Late Miocene Monte Capanne intrusion (Elba Island, Central Italy): constraints from magnetic fabric analyses, *Int. J. Earth Sci.*, *101*(3), 787–802, doi:10.1007/s00531-011-0701-z.

Cifelli, F., M. Mattei, H. Rashid, and J. Ghalamghash (2013), Right-lateral transpressional tectonics along the boundary between Lut and Tabas blocks (Central Iran), *Geophys. J. Int.*, *193*(3), 1153–1165, doi:10.1093/gji/ggt070.

Cowgill, E., A. Yin, J. R. Arrowsmith, W. X. Feng, and S. H. Zhang (2004), The Akato Tagh bend along the Altyn Tagh fault, northwest Tibet 1: Smoothing by vertical-axis rotation and the effect of topographic stresses on bend-flanking faults, *Geol. Soc. Am. Bull.*, *116*(11-12), 1423–1442.

Cullity, B. D. (1972), *Introduction to Magnetic Materials*, John Wiley & Sons, Hoboken, N. J.

Debacker, T. N., A. M. Hirt, M. Sintubin, and P. Robion (2009), Differences between magnetic and mineral fabrics in low-grade, cleaved siliciclastic pelites: A case study from the Anglo-Brabant Deformation Belt (Belgium), *Tectonophysics*, *466*(1-2), 32–46, doi:10.1016/j.tecto.2008.09.039.

Dedzo, M., A. Nédélec, A. Nono, and T. Njanko (2011), Magnetic fabrics of the Miocene ignimbrites from West-Cameroon: implications for pyroclastic flow source and sedimentation, *J. Volcanol. Geotherm. Res.*, *203*(3), 113–132.

Garcia-Lasanta, C., B. Oliva-Urcia, T. Roman-Berdiel, A. M. Casas, and F. Perez-Lorente (2013), Development of magnetic fabric in sedimentary rocks: insights from early compactional structures, *Geophys. J. Int.*, *194*(1), 182–199, doi:10.1093/gji/ggt098.

García-Lasanta, C., B. Oliva-Urcia, T. Román-Berdiel, A. M. Casas, and A. M. Hirt (2014), Understanding the Mesozoic kinematic evolution in the Cameros basin (Iberian Range, NE Spain) from magnetic subfabrics and mesostructures, *J. Struct. Geol.*, *66*, 84–101, doi:10.1016/j.jsg.2014.05.013.

Gautam, P., and W. Rösler (1999), Depositional chronology and fabric of Siwalik group sediments in Central Nepal from magnetostratigraphy and magnetic anisotropy, *J. Asian Earth Sci.*, *17*(5-6), 659–682, doi:10.1016/S1367-9120(99)00021-8.

Gee, J. S., L. Tauxe, and C. Constable (2008), AMSSpin: A LabVIEW program for measuring the anisotropy of magnetic susceptibility with the Kappabridge KLY-4S, *Geochem., Geophys. Geosyst.*, *9*, Q08Y02, doi:10.1029/2008GC001976.

Haerinck, T., R. Adriaens, T. N. Debacker, A. M. Hirt, and M. Sintubin (2013), Paramagnetic metamorphic mineral assemblages controlling AMS in low-grade deformed metasediments and the implications with respect to the use of AMS as a strain marker, *J. Geol. Soc.*, *170*(2), 263–280, doi:10.1144/jgs2012-062.

Henry, B., and L. Daly (1983), From qualitative to quantitative magnetic-anisotropy analysis - the prospect of finite strain calibration, *Tectonophysics*, *98*(3-4), 327–336, doi:10.1016/0040-1951(83)90300-1.

Hrouda, F. (2004), Problems in interpreting AMS parameters in diamagnetic rocks, *Geol. Soc. Spec. Publ.*, *238*, 49–59.

Hrouda, F., B. Henry, and G. Borradaile (2000), Limitations of tensor subtraction in isolating diamagnetic fabrics by magnetic anisotropy, *Tectonophysics*, *322*(3-4), 303–310, doi:10.1016/s0040-1951(00)00093-7.

Issachar, R., T. Levi, S. Marco, and R. Weinberger (2015), Anisotropy of magnetic susceptibility in diamagnetic limestones reveals deflection of the strain field near the Dead Sea Fault, northern Israel, *Tectonophysics*, *656*, 175–189, doi:10.1016/j.tecto.2015.06.02.

Izquierdo-Llavall, E., A. M. Casas-Sainz, and B. Oliva-Urcia (2013), Heterogeneous deformation recorded by magnetic fabrics in the Pyrenean Axial Zone, *J. Struct. Geol.*, *57*, 97–113, doi:10.1016/j.jsg.2013.10.005.

Jelinek, V. (1981), Characterization of the magnetic fabric of rocks, *Tectonophysics*, *79*(3-4), T63–T67, doi:10.1016/0040-1951(81)90110-4.

Jelinek, V. (1985), The physical principles of measuring magnetic anisotropy with the torque magnetometer, *Travaux Géophysiques*, *33*, 177–198.

Jelinek, V. (1995), Measuring anisotropy of magnetic susceptibility on a slowly spinning specimen-basic theory, *AGICO Print 10*.

LaBerge, R., M. Porreca, and M. Mattei (2009), Meandering flow of a pyroclastic density current documented by the anisotropy of magnetic susceptibility (AMS) in the quartz latite ignimbrite of the, *Tectonophysics*, *466*(1), 64–78.

Levi, T., and R. Weinberger (2011), Magnetic fabrics of diamagnetic rocks and the strain field associated with the Dead Sea Fault, northern Israel, *J. Struct. Geol.*, *33*(4), 566–578, doi:10.1016/j.jsg.2011.02.001.

Levi, T., R. Weinberger, T. Aïfa, Y. Eyal, and S. Marco (2006a), Injection mechanism of clay-rich sediments into dikes during earthquakes, *Geochem. Geophys. Geosyst.*, *7*, Q12009, doi:10.1029/2006GC001410.

Levi, T., R. Weinberger, T. Aïfa, Y. Eyal, and S. Marco (2006b), Earthquake-induced clastic dikes detected by anisotropy of magnetic susceptibility, *Geology*, *34*(2), 69–72.

Levi, T., R. Weinberger, and S. Marco (2014), Magnetic fabrics induced by dynamic faulting reveal damage zone sizes in soft rocks, Dead Sea basin, *Geophys. J. Int.*, *199*(2), 1214–1229, doi:10.1093/gji/ggu300.

Lüneburg, C. M., S. A. Lampert, H. D. Lebit, A. M. Hirt, M. Casey, and W. Lowrie (1999), Magnetic anisotropy, rock fabrics and finite strain in deformed sediments of SW Sardinia (Italy), *Tectonophysics*, *307*(1-2), 51–74, doi:10.1016/S0040-1951(99)00118-3.

Martin-Hernandez, F., and E. C. Ferre (2007), Separation of paramagnetic and ferrimagnetic anisotropies: A review, *J. Geophys. Res.*, *112*, B03105, doi:10.1029/2006JB004340.

Morin, F. J. (1950), Magnetic Susceptibility of αFe_ {2} O_ {3} and αFe_ {2} O_ {3} with Added Titanium., *Phys. Rev.*, *78*(6), 819.

Morris, A. (2000), Magnetic fabric and palaeomagnetic analyses of the Plio–Quaternary calc–alkaline series of Aegina Island, South Aegean volcanic arc, Greece, *Earth Planet. Sci. Lett.*, *176*(1), 91–105.

Morrish, A. H. (1994), *Canted Antiferromagnetism: Hematite*., World Scientific, 192 pp., Singapore.

Nathan, Y., and A. Flexer (1977), Clinoptilolite, paragenesis and stratigraphy, *Sedimentology*, *24*(6), 845–855.

Nye, J. F. (1957), *Physical Properties of Crystals: Their Representation by Tensors and Matrices*, Oxford university press, Oxford, U. K.

Oertel, G. (1983), The relationship of strain and preferred orientation of phyllosilicate grains in rocks—A review, *Tectonophysics*, *100*(1-3), 413–447, doi:10.1016/0040-1951(83)90197-X.

Oliva-Urcia, B., and T. Roman-Berdiel (2010), Tertiary compressional overprint on Aptian–Albian extensional magnetic fabrics, North-Pyrenean Zone, *J. Struct. Geol.*, *32*(3), 362–376.

Oliva-Urcia, B., J. Rahl, A. Schleicher, and J. Parés (2010), Correlation between the anisotropy of the magnetic susceptibility, strain and X-ray Texture Goniometry in phyllites from Crete, Greece, *Tectonophysics*, *486*(1), 120–131.

Oliva-Urcia, B., A. M. Casas, R. Soto, J. J. Villalaín, and K. Kodama (2011), A transtensional basin model for the Organyà basin (central southern Pyrenees) based on magnetic fabric and brittle structures, *Geophys. J. Int.*, *184*(1), 111–130, doi:10.1111/j.1365-246X.2010.04865.x.

Oliva-Urcia, B., A. M. Casas, M. J. Ramón, B. Leiss, E. Mariani, and T. Román-Berdiel (2012), On the reliability of AMS in ilmenite-type granites: an insight from the Marimanha pluton, central Pyrenees, *Geophys. J. Int.*, *189*(1), 187–203, doi:10.1111/j.1365-246X.2011.05355.x.

Oliva-Urcia, B., T. Román-Berdiel, A. M. Casas, M. F. Bógalo, M. C. Osácar, and C. García-Lasanta (2013), Transition from extensional to compressional magnetic fabrics in the Cretaceous Cabuérniga basin (North Spain), *J. Struct. Geol.*, *46*, 220–234, doi:10.1016/j.jsg.2012.09.001.

Ort, M., G. Orsi, L. Pappalardo, and R. Fisher (2003), Anisotropy of magnetic susceptibility studies of depositional processes in the Campanian Ignimbrite, Italy, *Bull. Volcanol.*, *65*(1), 55–72.

Owens, W. H., and E. H. Rutter (1978), The development of magnetic susceptibility anisotropy through crystallographic preferred orientation in a calcite rock, *Phys. Earth Planet. Inter.*, *16*(3), 215–222.

Özdemir, Ö., D. J. Dunlop, and T. S. Berquó (2008), Morin transition in hematite: Size dependence and thermal hysteresis, *Geochem., Geophys. Geosyst.*, *9*, Q10Z01, doi:10.1029/2008GC002110.

Ozisik, M. N. (1993), *Heat Conduction*, John Wiley & Sons, Hoboken, N. J.

Palmer, H., and W. MacDonald (1999), Anisotropy of magnetic susceptibility in relation to source vents of ignimbrites: empirical observations, *Tectonophysics*, *307*(1), 207–218.

Palchik, V., and Y. H. Hatzor (2002), Crack damage stress as a composite function of porosity and elastic matrix stiffness in dolomites and limestones, *Engineering Geology*, *63*(3), 233–245.

Parés, J. M., and B. A. van der Pluijm (2002), Phyllosilicate fabric characterization by Low-Temperature Anisotropy of Magnetic Susceptibility (LT-AMS), *Geophys. Res. Lett.*, *29*(24), 2215, doi:10.1029/2002GL015459.

Parés, J. M., and B. A. van der Pluijm (2014), Low-temperature AMS and the quantification of subfabrics in deformed rocks, *Tectonophysics*, *629*, 55–62, doi:10.1016/j.tecto.2014.03.005.

Parés, J. M., B. A. van der Pluijm, and J. Dinares-Turell (1999), Evolution of magnetic fabrics during incipient deformation of mudrocks (Pyrenees, northern Spain), *Tectonophysics*, *307*(1-2), 1–14.

Pennec, J. L., Y. Chen, and H. Diot (1998), Interpretation of anisotropy of magnetic susceptibility fabric of ignimbrites in terms of kinematic and sedimentological mechanisms: An Anatolian case-study, *Earth Planet. Sci. Lett.*, *157*(1), 105–127.

Petronis, M., and J. Geissman (2009), Anisotropy of magnetic susceptibility data bearing on the transport direction of mid-tertiary regional ignimbrites, Candelaria Hills area, West-Central Nevada, *Bull. Volcanol.*, *71*(2), 121–151.

Porreca, M., and M. Mattei (2003), Magnetic fabric and implications for pyroclastic flow and lahar emplacement, Albano maar, Italy, *J. Geophys. Res.*, *108*(B5), 2264, doi:10.1029/2002JB002102.

Rochette, P., C. Aubourg, and M. Perrin (1999), Is this magnetic fabric normal? A review and case studies in volcanic formations, *Tectonophysics*, *307*(1), 219–234.

Santolaria, P., A. M. Casas, and R. Soto (2015), Anisotropy of magnetic susceptibility as a proxy to assess internal deformation in diapirs: case study of the Naval salt wall (Southern Pyrenees), *Geophys. J. Int.*, *202*(2), 1207–1222, doi:10.1093/gji/ggv231.

Schmidt, V., D. Gunther, and A. M. Hirt (2006), Magnetic anisotropy of calcite at room-temperature, *Tectonophysics*, *418*(1-2), 63–73, doi:10.1016/j.tecto.2005.12.019.

Schmidt, V., A. M. Hirt, P. Rosselli, and F. Martin-Hernandez (2007), Separation of diamagnetic and paramagnetic anisotropy by high-field, low-temperature torque measurements, *Geophys. J. Int.*, *168*(1), 40–47, doi:10.1111/j.1365-246X.2006.03202.x.

Soto, R., A. M. Casas-Sainz, J. J. Villalain, and B. Oliva-Urcia (2007), Mesozoic extension in the Basque-Cantabrian basin (N Spain): Contributions from AMS and brittle mesostructures, *Tectonophysics*, *445*(3-4), 373–394, doi:10.1016/j.tecto.2007.09.007.

Soto, R., J. C. Kullberg, B. Oliva-Urcia, A. M. Casas-Sainz, and J. J. Villalaín (2012), Switch of Mesozoic extensional tectonic style in the Lusitanian basin (Portugal): Insights from magnetic fabrics, *Tectonophysics*, *536-537*, 122–135, doi:10.1016/j.tecto.2012.03.010.

Soto, R., E. Beamud, B. Oliva-Urcia, and E. Roca (2014), Applicability of magnetic fabrics in rocks associated with the emplacement of salt structures (the Bicorb–Quesa and Navarrés salt walls, Prebetics, SE Spain), *Tectonophysics*, *629*, 319–334.

Verwey, E. J. W. (1939), Electronic Conduction of Magnetite (Fe3O4) and its Transition Point at Low Temperatures, *Nature*, *144*(3642), 327–328. [Available at http://www.nature.com/nature/journal/v144/n3642/abs/144327b0.html, last accessed 7 July 2014.]

Wang, X., J. Roberts, and P. Schmidt (2001), Flow directions of Carboniferous ignimbrites, southern New England Orogen, Australia, using anisotropy of magnetic susceptibility, *J. Volcanol. Geotherm. Res.*, *110*(1), 1–25.

Zanella, E., G. De Astis, and P. Dellino (1999), Magnetic fabric and remanent magnetization of pyroclastic surge deposits from Vulcano (Aeolian Islands, Italy), *J. Volcanol. Geotherm. Res.*, *93*(3), 217–236.